

## BENDING STRENGTH OF SOLDER JOINTS AS A FUNCTION OF JOINT LENGTH

Saeed Akbari, Amir Nourani, Jan K. Spelt  
University of Toronto  
Toronto, ON, Canada  
spelt@mie.utoronto.ca

### ABSTRACT

The effect of the joint length on the fracture of copper-solder-copper joints were investigated using double-cantilever-beam (DCB) specimens of various joint lengths. It was found that for solder joints shorter than a certain characteristic length the strength increased with increasing joint length. This characteristic length was found numerically using a finite element model to plot the maximum peel stress of the solder joint versus the joint length. The length at which the plot reaches a plateau was considered as the characteristic length. Characteristic lengths obtained from experiment and finite element analysis were in close agreement, indicating the validity of the numerical method. The practical importance of the characteristic length is that solder joints longer than the characteristic length have a maximum peel stress that remains unchanged with joint length, causing the joint strength to become independent of the joint length. In other words, the use of joints longer than the characteristic length provides no additional strength to the joint.

Key words: SAC solder, copper, joint length, peel stress, finite element analysis

### INTRODUCTION

Solder joints provide critical links in many assemblies, joining various substrates with different bending stiffnesses. For example, in first level packaging they join chips and substrates, or in board-level packaging they connect components and printed circuit boards (PCBs) [1-2]. In microelectronics assemblies most solder joints are used either in the form of closely-spaced discrete joints, such as ball grid arrays, where load sharing occurs, or as relatively large, isolated joints such as in heat sinks or power modules [3-4].

The length of these solder joints ranges from approximately 100  $\mu\text{m}$  to several centimeters, and their thickness ranges from approximately 100  $\mu\text{m}$  to about 500  $\mu\text{m}$  [4-5]. In spite of the wide range of solder joint lengths in common microelectronics applications, only a relatively small number of published studies have examined the effect of joint length on joint strength. The relatively few studies which have investigated this relationship have often used copper-solder-copper tensile specimens to investigate the effect of the thickness and length of solder layers on the joint tensile strength [6-9],

as shown in Fig. 1. For example, Yin et al. [7] used solder joints between copper wires to investigate the effect of the thickness and diameter of a Sn3.0Ag0.5Cu (SAC 305) solder layer (Fig. 1(a)). For joints ranging in thickness from 75  $\mu\text{m}$  to 525  $\mu\text{m}$  and in diameter from 200  $\mu\text{m}$  to 575  $\mu\text{m}$  it was shown that a decrease in the thickness or diameter induced higher triaxial stresses in the solder layer resulting in increases up to approximately 100% in the ultimate tensile strength.

However, tests designed to predict the strength of solder joints in a particular application must be able to reflect the nature of the actual loading conditions and the resulting stress states. PCB or substrate bending is one of the main reasons for the mechanical failure of solder joints; therefore, tensile test specimens such as those in Fig. 1 do not represent the dominant stress states found in many practical loading conditions.

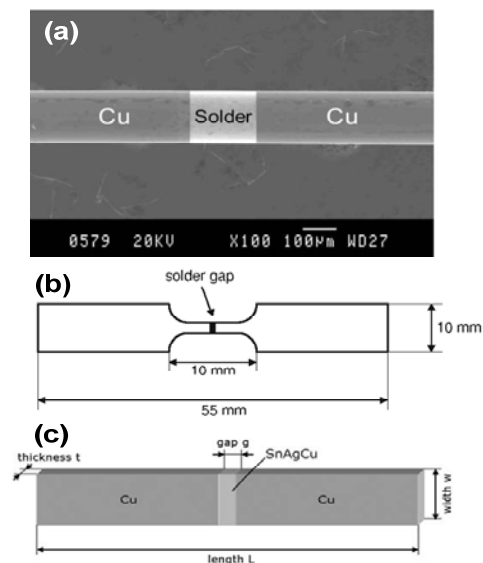


**Fig. 1.** Cu-solder-Cu tensile specimens used by (a) Yin [7] (b) Zimprich [8] (c) Cugnoni [9]

The major objective of the present study was to assess the effect of solder joint length on the fracture strength. Experiments were performed using a bending-type test specimen, the double cantilever beam (DCB), to measure the mode-I fracture strength of solder joints of various

lengths. Since solder fracture is dominated by substrate peel deformation in a DCB, a finite element model was used to calculate the maximum peel stress of the solder joint as a function of the joint length. The experimental strength data were then compared with the peel stress predictions of the finite element model to reveal how joint length related to joint strength.

## EXPERIMENT

Cu-solder-Cu double-cantilever-beam (DCB) specimens were prepared with a continuous solder joint of different lengths (Fig. 2) made with Sn3.0Ag0.5Cu (SAC 305) solder with a thickness of 127  $\mu\text{m}$ . The arms of the DCB specimens were fabricated from copper bars (C110 alloy) with a square cross-section (12.7  $\times$  12.7 mm).

The surface of the copper bars to be soldered were polished using an ultra-fine silicon carbide/nylon mesh abrasive to produce a repeatable surface roughness of  $Ra=1 \mu\text{m}$ , which is very similar to that on the copper pads of commercial PCBs.

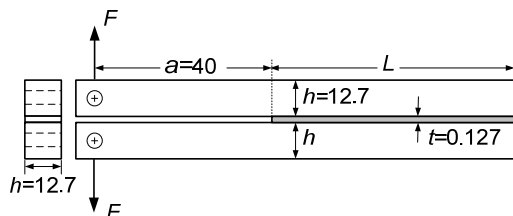


**Fig. 2.** Schematic of the Cu-solder-Cu DCB specimen. Dimensions in mm. Not to scale.

The copper bars were cleaned with acetone, and were then masked with Kapton tape to produce specimens having six different lengths ( $L=2, 5, 10, 15, 30,$  and  $50$  mm). The Kapton tape formed a smooth square local geometry at the end of the solder layer.

In order to control the thickness of the solder layer, two 127  $\mu\text{m}$  diameter steel wires were placed between the copper bars. The copper bars were heated on a hot plate, and a flux-cored SAC305 solder wire (Kester Inc., USA) was applied to the copper surfaces to be soldered and the joint was closed and left for 120\_s (i.e. the time-above-liquidus) before being transferred to a small wind tunnel to achieve a cooling rate of 1.4-1.6  $^{\circ}\text{C}/\text{s}$ , which is typical of microelectronic manufacturing.

Excess solder that flowed from the edges of the joint was wiped away immediately using a piece of cloth, so no machining of the sides of the DCB was required before testing. The holes for the loading pins of the DCB specimen were drilled in the copper bars. Fracture experiments were performed at a constant cross-head speed of 4.23 mm/s. A finite element model showed that the corresponding opening strain rate at the end of the solder layer was 0.22  $\text{s}^{-1}$ . Five specimens were tested for each joint length. All DCB specimens were fracture tested one day after fabrication.

## FINITE ELEMENT MODEL

It was hypothesized that the solder peel stress (tensile stress normal to the copper) was responsible for crack

initiation. A finite element model (FEM) of the DCB joint of Fig. 2 was used to calculate the peel stress distribution of the solder layer. Two-dimensional, 8-node quadratic elements (Plane183, ANSYS®15, Ansys Inc, Canonsburg, PA), were used to model the solder joint and copper bars. The dimensions of the solder layer and the copper bars in the DCB joints implied that plane stress and plane strain conditions were appropriate for the copper bars and the solder layer, respectively (Fig. 3).

Both the copper bars and the solder were modeled as isotropic, linear-elastic materials with the material properties of Table 1. As will be shown in Results section, the load-displacement curve of the fracture experiments was completely linear until final fracture, so plastic deformation was negligible.

At least 15 elements were used across the thickness of the solder layer to capture the steep stress gradients, especially in the end regions. Mesh independence was established by re-meshing with smaller elements. The rate of displacement of the ends of the specimen at the location of the loading pins was used to calculate the local rate of change of the solder layer thickness and the opening strain rate of the solder layer, which was 0.22  $\text{s}^{-1}$  in all of the tests. Using the measured fracture load, the peel stress distribution in the mid-plane of the solder layer was calculated with the FE model.

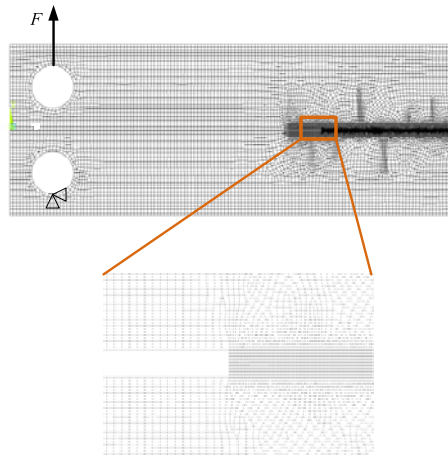


**Fig. 3.** Finite element model of the DCB test specimen used to calculate peel stresses in solder layer.

**Table 1.** Mechanical properties used in the FE analysis [10].

	Young's Modulus (GPa)	Poisson's ratio
Copper	124	0.35
SAC305	41	0.4

## RESULTS

### Solder Peel Stress

Figures 4 and 5 show the peel stress distribution along the mid-plane of the solder layer of mode-I DCB specimens with solder lengths of 50 mm and 5 mm, respectively. Since the main interest was in the distribution of the peel stress rather than its magnitude, the force applied to both

arms of the DCB was arbitrarily set as  $F=200$  N, which was smaller than the measured failure force for the 50 mm joint (presented below). In the 50 mm joint, the peel stress was maximum at the left edge of the joint, decreased within a short distance to become compressive, and then increased to zero. In the 5 mm joint, the peel stress was positive in the first half of the length, and negative in the second half.

The strain rate used in the present experiments was  $0.22\text{ s}^{-1}$ , where the yield strength of SAC305 solder is  $S_y=60$  MPa [11]. Since a linear elastic finite element model was used, the maximum von Mises stress at the solder layer of a Cu-solder-Cu DCB specimen could be larger than the yield strength. However, the purpose of the peel stress calculations was to find the characteristic length,  $L_{cr}$ , from the changes in the stress distribution along the joint; hence, the absolute values of the stresses were not of interest. It was confirmed that solder plasticity had no effect on  $L_{cr}$  by modeling the solder layer as an elastic-perfectly plastic material. As with the elastic model,  $L_{cr}$  was assumed to be the joint length where the maximum peel stress reached a constant value. It was seen that the calculation of  $L_{cr}$  was unaffected by consideration of solder plasticity, and the present results were identical to those obtained using an elastic-plastic finite element model.

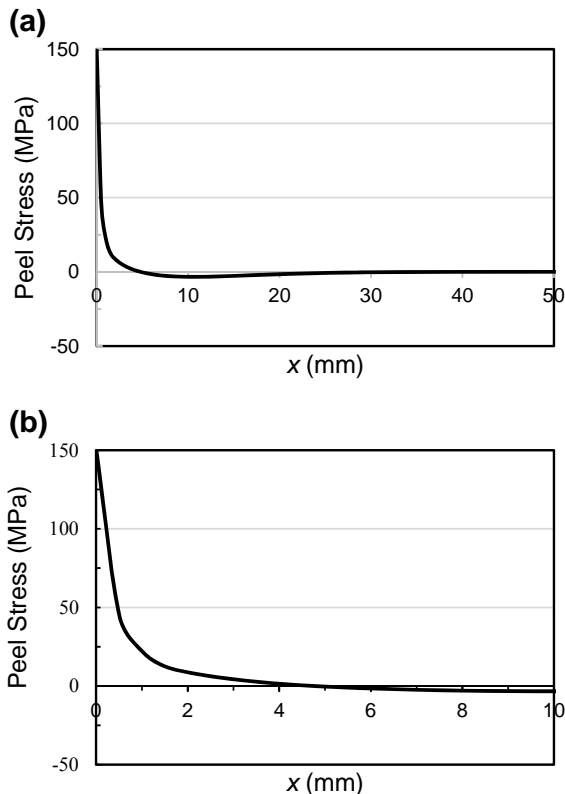


**Fig. 4.** Solder peel stress predictions along the mid-plane of a 50 mm long mode I DCB joint with load  $F=200$  N: (a) peel stress distribution along the entire solder layer and (b) peel stresses near the left edge of the solder layer.

In order to find the characteristic length,  $L_{cr}$ , of the DCB of Fig. 2, the maximum solder peel stress was plotted

versus the joint length using an arbitrary constant applied force, as shown in Fig. 6 for  $F=200$  N. Since a linear elastic model was used to determine these stress distributions, the joint characteristic length where the maximum peel stress becomes constant ( $L_{cr}$ ) was independent of the applied load. Figure 6 shows that as the joint became shorter, the maximum peel stress increased rapidly. The prediction of  $L_{cr}$  from the finite element analysis (Fig. 6) was approximately 15 mm.

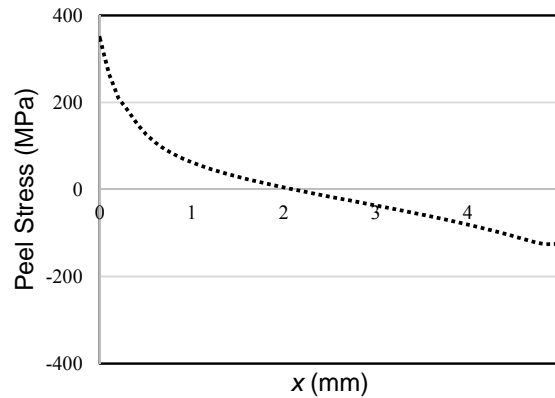


**Fig. 5.** Solder peel stress predictions along the mid-plane of a 5 mm long mode I DCB joint with load  $F=200$  N.

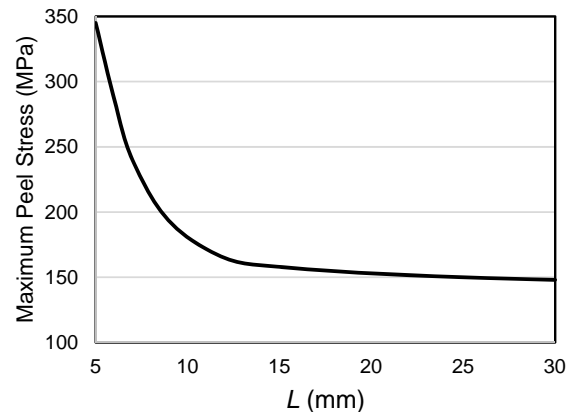


**Fig. 6.** Maximum predicted solder peel stress at the mid-plane of solder layer for different solder joint lengths and  $F=200$  N.

### Experimental Results

Figure 7 shows a typical load–displacement response for a DCB fracture test of a 30 mm long joint, with data points recorded at a sampling rate of 1 kHz in order to accurately measure the maximum load. The fracture load was evident as a sudden drop in the recorded load cell output. The initial nonlinearity in the curve was due to the take-up of the clearance in the pin used to load the DCB arm.

In fracture tests of adhesive and solder joints using DCBs, the onset of nonlinearity in the load-displacement curve is considered a measure of adhesive or solder plastic deformation [12-13]. Figure 7 illustrates that the load-displacement curves in the present experiments were completely linear until final fracture, so plastic deformation and R-curve crack-tip toughening were negligible [10]. Similar behavior was observed in all of

the tests, regardless of joint length. Therefore, the maximum measured force was considered to coincide with both crack initiation and final fracture. These maximum loads were used in the FE model to calculate stress distributions in the solder layer. The absence of significant R-curve behavior contrasts with the toughening reported by Nadimpalli and Spelt [10] using SAC305 solder and similar specimens when tested under quasi-static conditions (strain rate of  $6 \times 10^{-5} \text{ s}^{-1}$ ). This difference was due to the much higher strain rate used in the present experiments ( $0.22 \text{ s}^{-1}$ ), which caused the joint to undergo fast fracture before a crack tip damage zone could develop and grow to generate R-curve behavior [10].

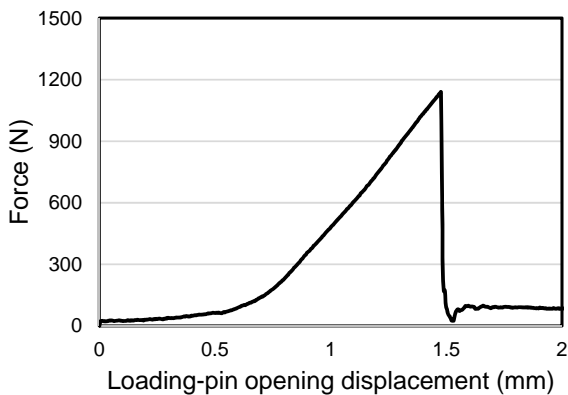


**Fig. 7.** Typical load–displacement response for a mode I DCB specimen with a 30 mm long solder layer.

Figure 8 shows the measured fracture loads for the DCB specimens of different solder layer lengths. As expected from the maximum peel stress predictions of Fig. 6, for relatively short solder joints the fracture load increased with joint length up to approximately a joint length of 13–15 mm, after which it remained constant. The *t*-test showed that the difference between the average fracture load values for relatively long joints (15, 30, and 50 mm) was statistically insignificant at the 95% confidence level. Therefore, based on the measured joint strengths,  $L_{cr}$  was approximately 15 mm, which agrees well with the FEM prediction of Fig. 6.

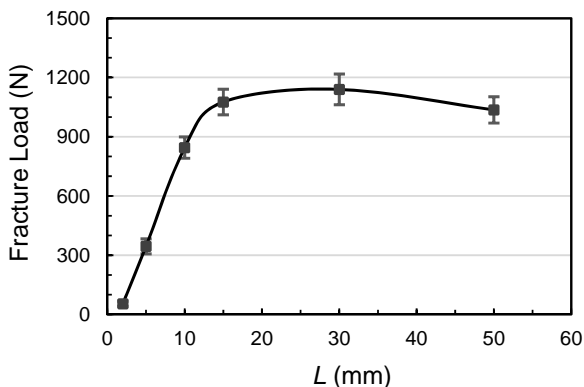


**Fig. 8.** Fracture load of DCB specimens under mode I loading for different joint lengths. Error bars indicate  $\pm 1$  standard deviation based on 5 repeat experiments at each length.

An important practical implication of these results is that, for each joint configuration under various loads, a characteristic length can be defined based on the change of the maximum peel stress. The use of joints longer than the characteristic length provides no additional strength to the joint.

### Fracture Surface Analysis

In all specimens, the crack grew quickly along one interface. Figure 9(a) shows that the typical fracture surface of the tested specimens was smooth and macroscopically flat, which is a characteristic of solder fracture surface at intermediate and high strain rates [14–16].

The microstructure of the fracture surfaces was characterized using scanning electron microscopy (SEM) and energy-dispersive X-ray spectroscopy (EDX). The solder fracture surfaces displayed a mixture of brittle and ductile features. IMC or solder-IMC crack paths were characteristic of brittle fracture, displaying less tin and more copper, indicating a greater proportion of IMC failure.

The brittle fracture of  $\text{Cu}_6\text{Sn}_5$  grains leaves flat hexagonal features on the fracture surface (Fig. 9(b)), as confirmed by the EDX spectrum (note the Cu peak in Fig. 9(d)). The areas of relatively uniform, fine-grained roughness are typical of brittle decohesion along the solder-IMC interface [10, 14–16]. These brittle failure modes in general indicate the initial failure of the solder at the ends of the layer [17].

Ductile fracture through the solder layer created dimples with round shapes (Fig. 9(b)), which was confirmed by the EDX spectrum (Fig. 12(c)). This ductile fracture generally corresponded to crack propagation in the central portions of the solder layer after the peak load had initiated cracking at the end of the layer [17].

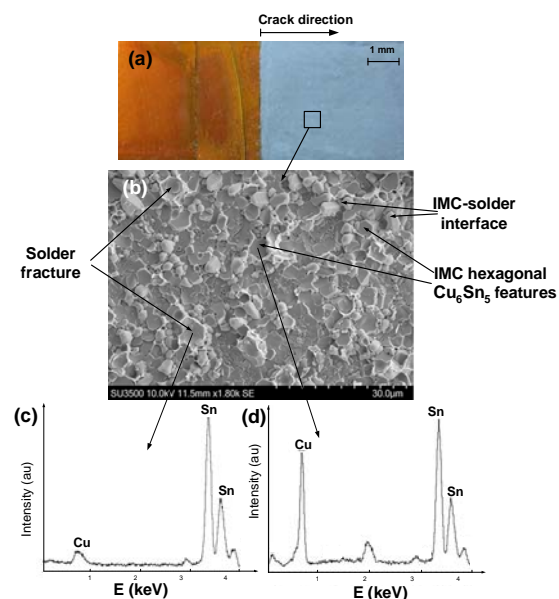


**Fig. 9.** (a) A typical fracture surface. Crack direction is from left to right. (b) SEM micrograph of the fracture surface, (c-d) EDX spectra of the fracture surface.

These results suggest that the crack propagated close to the more highly-strained substrate (the upper substrate in Figs. 2 and 3) above the interface between the solder and IMC layer. No significant difference was observed between the fracture surfaces of joints with various lengths.

### Case Study: Chip Resistor

The concept of a characteristic joint length is applicable to the solder joints used in surface-mount microelectronics assemblies. For example, Fig. 10 shows a chip resistor with solder joints of length  $L_2$  at either end. When the PCB is subject to bending, the resulting peel stresses in the solder layer can cause solder cracking. For a typical chip resistor with the material properties and dimensions of Table 2, a finite element model was used to determine the maximum peel stress in the solder layer using the boundary conditions and applied load,  $F$ , of Fig. 10. The distance between the loading point and the edge of the chip,  $L_F$ , was taken to be 4.88 mm in this example.

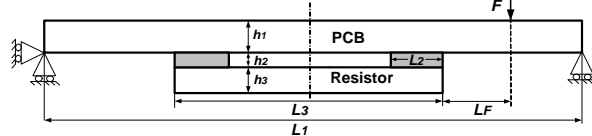


**Fig. 10.** Schematic of a chip resistor assembly with loading conditions.

**Table 2.** Dimensions and material properties of a typical chip resistor [18]. Symbols defined in Fig. 10.

Layers	$h$ (mm)	$L$ (mm)	$E$ (GPa)	$\nu$
PCB (1)	1.23	13	22	0.28
Solder (2)	0.12	Variable	41	0.4
Resistor (3)	0.65	6.5	131	0.3

Figure 11 shows that the maximum peel stress became independent of the solder joint length,  $L_2$ , at approximately 1 mm. Therefore, it can be postulated that joints longer than this characteristic length of 1 mm are not stronger than a 1 mm long joint when subject to such bending loads that create peel stresses.

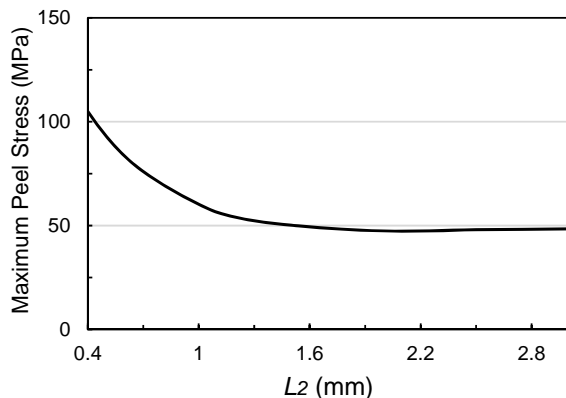


**Fig. 11.** FEM predictions of the maximum peel stress as a function of the length of the right-hand solder joint in Fig. 10. Stress calculated at the mid-plane on the right side of

the joint. Properties of Table 2 with applied load  $F=2$  N/mm.

### CONCLUSIONS

The fracture strength of mode-I copper DCB specimens were measured with SAC305 solder joints of various lengths. Joint strength increased with increasing solder length before reaching a plateau value of constant strength. The corresponding finite element model showed that the maximum peel stress became independent of the length of the solder layer beyond a characteristic length which was very close to the solder length corresponding to the initiation of the measured joint-strength plateau. This supported the hypothesis that solder joints reach a maximum strength at the characteristic solder length, and that further increases in length do not result in stronger joints.

The concept of the characteristic length was illustrated in a hypothetical chip resistor assembly loaded by board bending. The characteristic length of a typical chip resistor solder joint was predicted to be about 1 mm, as determined from the finite element predictions of the maximum solder peel stress as a function of the joint length.

### ACKNOWLEDGEMENTS

The authors are thankful to BlackBerry and the Natural Sciences and Engineering Research Council of Canada for their financial support. The authors would like to thank Dr. Gene Burger and Dr. Bev Christian of BlackBerry for their valuable advice and technical support.

### REFERENCES

- [1] An T, Qin F. Effects of the intermetallic compound microstructure on the tensile behavior of Sn3.0Ag0.5Cu/Cu solder joint under various strain rates. *Microelectronics Reliability*. 2014;54:932–938
- [2] Shen J, Zhai D, Cao Z, Zhao M, Pu Y. Fracture behaviors of Sn-Cu intermetallic compound layer in ball grid array induced by thermal shock. *J. Electronic Materials*. 2014;43:567-575.
- [3] Dugala F, Ciappab M. Study of thermal cycling and temperature aging on PbSnAg die attach solder joints for high power modules. *Microelectronics Reliability* 2014;54:1856–1861.
- [4] Han C, Oh C, Park N, Hong W. Creep lifetime prediction of solder joint for heat sink assembly. *Microelectronics Reliability* 2010;50:1645–1649.
- [5] Nadimpalli SPV, Spelt JK. Effect of geometry on the fracture behavior of lead-free solder joints. *Eng. Fract. Mechanics* 2011;78:1169-1181.
- [6] Ranieri JP, Lauten FS, Avery DH. Plastic constraint of large aspect ratio solder joints. *J. Electronic Materials* 1995; 24:1419-1426.
- [7] Yin, L.M., Zhang, X.P., Lu, C. Size and volume effects on the strength of microscale lead-free solder joints. *J. Electronic Materials*, 2009;38:2179-2185.
- [8] Zimprich P, Saeed U, Weiss B, Ipser H. Constraining effects of lead-free solder joints during stress relaxation. *J. Electronic Materials* 2009;38:392-399.
- [9] Cugnoni J, Botsis J, Sivasubramaniam V, Janczak-Rusch J. Experimental and numerical studies on size and constraining effects in lead-free solder joints.

- Fatigue and Fracture of Eng. Materials and Structures 2007;30:387–399.
- [10]Nadimpalli SPV, Spelt JK. R-curve behavior of Cu–Sn3. 0Ag0. 5Cu solder joints: Effect of mode ratio and microstructure. Materials Sci. and Eng.: A 2010;527:724-734.
- [11]Lall P, Shantaram S, Locker D. High strain rate properties of SAC105 and SAC305 lead-free alloys after extended high temperature storage. SMTA Journal 2014;27:13-27.
- [12]ISO, Standard test method for the mode I interlaminar fracture toughness,  $G_{IC}$ , of unidirectional fibre-reinforced polymer matrix composites. ISO15024, 2001.
- [13]Blackman BRK, Kinloch AJ, Parasachi M, Teo WS. Measuring the mode I adhesive fracture energy,  $G_{IC}$ , of structural adhesive joints: the results of an international round-robin. Int. J. Adhes Adhes 2003;23:293–305.
- [14]Nourani A, Spelt JK. Effect of solder alloy, aging and TAL on high strain-rate fracture of lead-free solder joints. SMTA Int. Conf. Proc. (2015).
- [15]Nourani A, Spelt JK. Effect of processing parameters on fracture toughness of lead-free solder joints. Eng. Fract. Mech. 2015;142:64.
- [16]Nourani A, Spelt JK. Combined effect of strain-rate and mode-ratio on the fracture of lead-free solder joints. Mater. Des. Accepted.
- [17]Lai YS, Chang HC, Yeh CL. Evaluation of solder joint strengths under ball impact test. Microelectron. Reliab. 2007;47:2179-2186.
- [18]Qi Y, Ghorbani HR, Spelt JK. Thermal fatigue of SnPb and SAC resistor joints: Analysis of stress-strain as a function of cycle parameters. IEEE Trans. Adv. Packag. 2006;43:690–700.